Penerbit Akademia Baru

Journal of Advanced Research in Fluid Mechanics and Thermal Sciences

Journal homepage: www.akademiabaru.com/arfmts.html
ISSN: 2289-7879

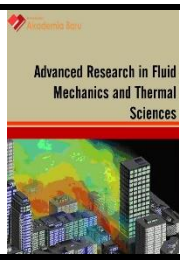

An Analysis of Blood Pressure Waveform using Windkessel Model for Normotensive and Hypertensive Conditions in Carotid Artery

Open Access

Muhammad Sufyan Amir Paisal[1,*], Ishkrizat Taib[1], Al Emran Ismail[1,♣], Ahmad Mubarak Tajul Arifin[1], Nofrizalidris Darlis[2]

[1] Faculty of Mechanical and Manufacturing Engineering (FKMP), Universiti Tun Hussein Onn Malaysia (UTHM), Batu Pahat, 86400, Malaysia
[2] Faculty of Engineering Technology (FTK), Universiti Tun Hussein Onn Malaysia (UTHM), Batu Pahat, 86400, Malaysia

ARTICLE INFO

Article history:
Received 12 December 2018
Received in revised form 4 April 2019
Accepted 1 May 2019
Available online 10 May 2019

ABSTRACT

Arterial blood pressure waveforms of common carotid artery (CCA) at different physiological conditions are rarely modeled and compared by the previous study. The artery in the cardiovascular system has been known to be analogous with the electrical circuit. Therefore, this study aims to assess and have a full understanding onto the blood pressure waveforms in CCA at different physiological of normotensive and hypertensive conditions invasively. A 4-element Windkessel model is used to obtained the blood pressure from the existing velocity waveforms at three physiological conditions namely as Normal Blood Pressure (NBP), Pre-Hypertension (PH) and Hypertension Stage One (HS1). The results have shown that the blood pressure waveforms are successfully simulated and achieve acceptable agreement with the previous study. The simulated blood pressure waveforms in CCA obtain different patterns which correspond to their velocity waveform. Thus, the augmentation index AI of the pressure waveforms obtained by NBP, PH, and HS1 conditions gave values about 9.77%, 14.94% and 25.17%, respectively. Since these values are acceptable with previous study, the 4-element Windkessel model is reliable in predicting the arterial blood pressure waveform that associate with cardiovascular disease.

Keywords:
carotid artery, pressure waveform, normotensive, hypertensive, Windkessel model, 4-element

1. Introduction

Arterial blood pressure waveform plays the main role to describe the activity of the heart which affecting the particular artery in systole and diastole of each cardiac cycle [1,2]. Instead of using Doppler ultrasound method and sphygmomanometer, a mathematical model namely as Windkessel model is easily able to simulate the cardiac cycles of the heart [3-5]. The mathematical model is

* *Corresponding author.*
E-mail address: muhammadsufyanamir@gmail.com
♣ *Corresponding author.*
E-mail address: al_emran@hotmail.com

derived from electrical circuit analogies where current represents the arterial blood flow and voltage represents the arterial blood pressure as illustrated in Figure 1 [6-14].

Previously, the Windkessel model was introduced with only two elements which consist of peripheral resistance and capacitance. However, this model produces unrealistic aortic pressure waveform due to lack of systemic input impedance. Later on, characteristic impedance is included as the third element of the three-element Windkessel model to overcome the problem. However, the capacitance tends to be overestimated and the characteristic impedance tends to be underestimated. The Windkessel model is improved as four-element by implying the inertia of the arterial cardiovascular system [15]. These Windkessel models can be seen in Figure 2 displaying their own analogous electrical diagram [16]. Although the position of inductor in the four-element Windkessel model has been modified for an improvement [17], the general four-element model still performs well in simulating the blood flow in congenital heart diseases [18,19].

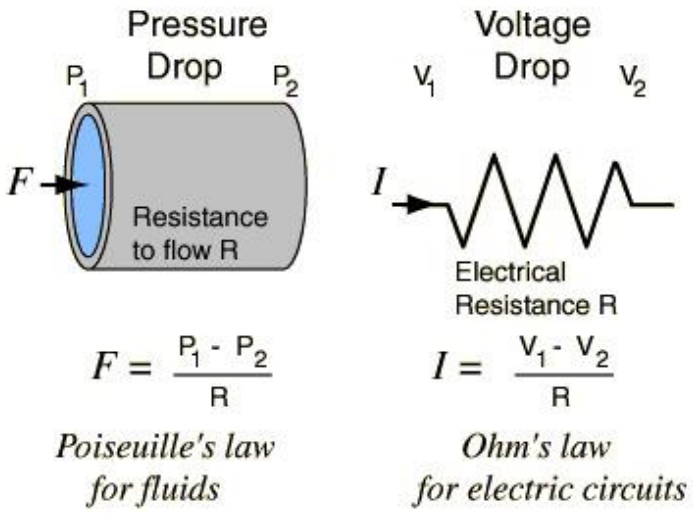

Fig. 1. Analogy of blood flow to the electrical circuit [7]. R represents resistor; *I* represents current; *F* represents flow; P_1 and P_2 represent pressures; V_1 and V_2 represent voltages

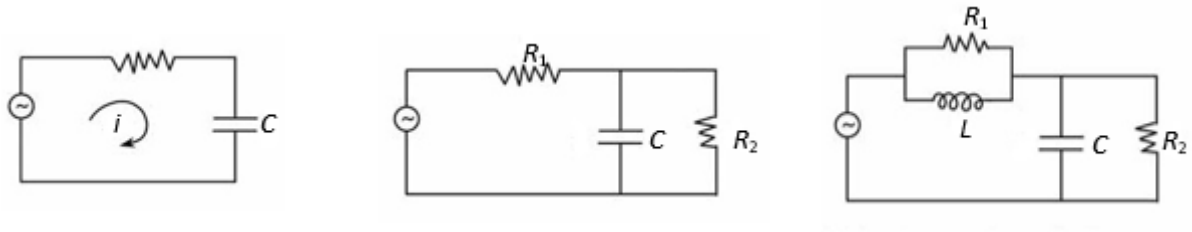

(a) (b) (c)

Fig. 2. Electrical circuit of Windkessel model for (a) 2-element, (b) 3-element and (c) 4-element [16]. *R*, R_1 and R_2 are resistors; *i* is current; *L* is conductor; *C* is capacitor

On the other hand, the blood pressure waveform enlarges from the central aorta to the peripheral artery as seen in Figure 3 [20]. The pressure waveform of the central aorta has been widely studied as displayed in Figure 4 [21]. However, the peripheral artery such as carotid artery is hardly studied in detail for its reflected pressure time, pulse pressure, ejection duration and the augmented pressure at different physiological conditions.

Thus, it triggers the present study to use the general four-element Windkessel model in assessing the hemodynamic pressure waveform with different physiological conditions consisting of normotensive and hypertensive blood flow. In addition, hypertensive physiological condition of blood in carotid artery is rarely simulated through Windkessel model and compared with the normotensive condition. Therefore, this study aims to have a full understanding on the activity of blood pressure waveform that happen in normotensive and hypertensive carotid artery.

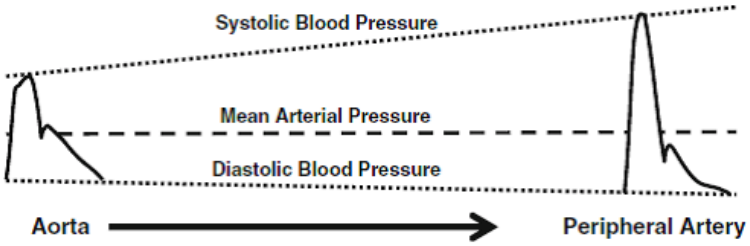

Fig. 3. Enlargement in blood pressure waveform from the central aorta to the periphery of the arterial system [20]

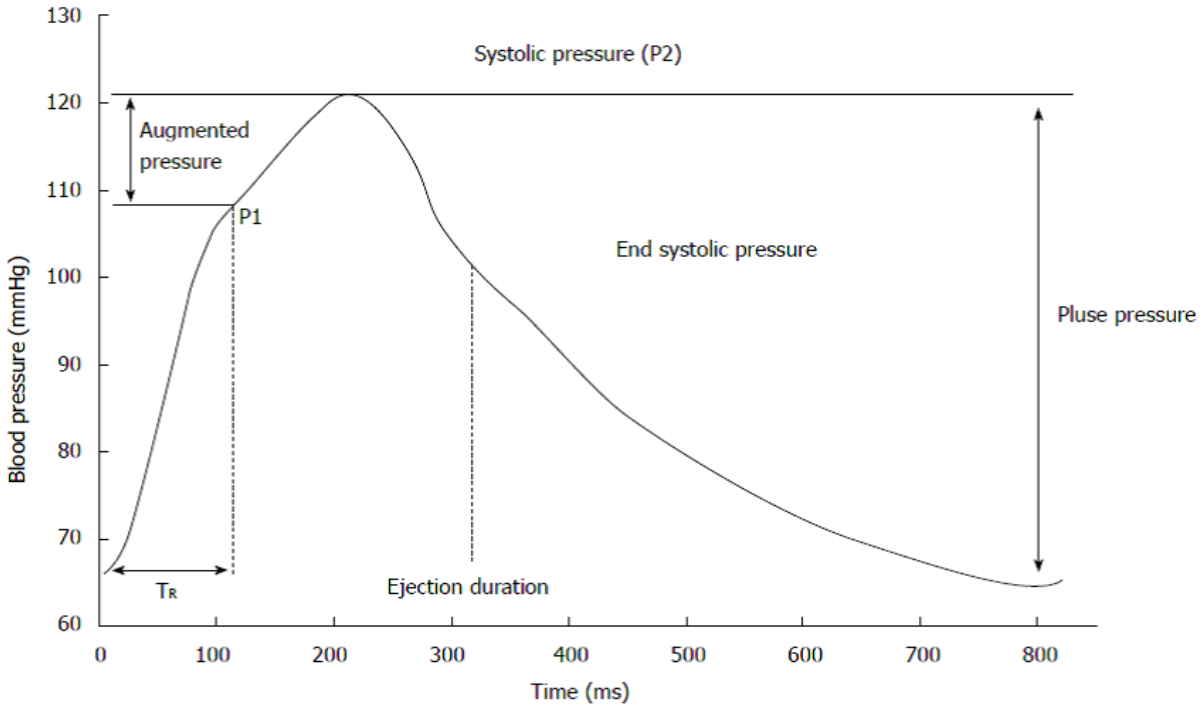

Fig. 4. Central aorta pressure waveform showing the time of reflected pressure wave (T_R), first systolic pressure (P1), second systolic pressure (P2), pulse pressure and augmented pressure [22]

2. Methodology

The simulation of blood pressure waveform by applying Windkessel 4-element model is done on numerical computation software called as MATLAB (Mathworks, Natick, Massachusetts, United States). Further sub-chapters describe the input data, blood parametric assumptions and the properties of carotid artery that used in the mathematical formulations to obtain the desired pressure waveform by using the software. An actual measured pressure waveform of carotid artery is then compared with the simulated pressure waveform to ensure the present study is valid.

2.1 Blood Velocity Waveform as Input for the Mathematical Model

The input data using velocity waveforms of blood in carotid artery are based on a study by Azhim *et al.,* consisting of three physiological conditions which namely as Normal Blood Pressure (NBP), Pre-Hypertension (PH) and Hypertension Stage 1 (HS1). As shown in Figure 5, the velocity waveform of NBP condition represents the systolic and diastolic blood pressure of heart about 117/71 mmHg. On the other hand, the velocity waveform of carotid artery in PH condition represents 124/81 mmHg while HS1 condition represents 148/96 mmHg for heart blood pressure. These velocity waveforms are obtained from young adult where the age is ranged from 31 to 37 years old [23].

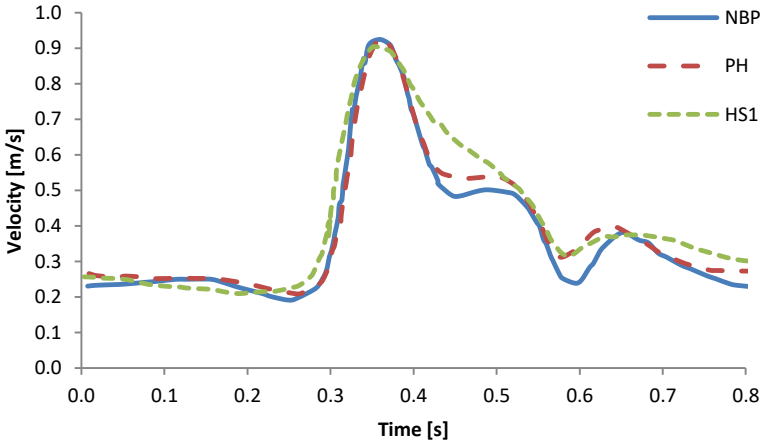

Fig. 5. Velocity waveform of carotid artery at physiological flow condition of NBP, PH and HS1[23]

By using a curve fitting toolbox in MATLAB, the velocity (m/s) waveforms were approximated as Fourier series $V(t)$ in term of time t as displayed in Eq. (1). This equation is able to mimic the continuous cardiac cycle of the waveform. Thus, the empirical variables for the Fourier series were demonstrated as seen in Table 1.

$$V(t) = a_0 + \sum_{n=1}^{8} a_n \cos(nt\omega) + \sum_{n=1}^{8} b_n \sin(nt\omega) \tag{1}$$

On the other hand, the mentioned systolic and diastolic blood pressures can be represented as mean arterial pressure (MAP) for entire cardiovascular system for each physiological condition by using Eq. (2) [20]. P_d represents diastolic blood pressure while P_s represents systolic blood pressure. Therefore, the MAP for NBP, PH and HS1 conditions obtained about 86.333 mmHg, 95.333 mmHg and 113.333 mmHg, respectively.

$$\mathrm{MAP} = \mathrm{P_d} + \frac{1}{3}\left(\mathrm{P_s} - \mathrm{P_d}\right) \tag{2}$$

Table 1
Empirical Variables of Fourier Series for each Blood Physiological Condition

Parameter	Blood condition		
	NBP	*PH*	*HS1*
ω	8.302	8.607	7.878
a_0	0.3782	0.4009	0.4119
a_1	-0.1812	-0.1616	-0.2122
a_2	0.1276	0.1073	0.1478
a_3	-0.08981	-0.08038	-0.06878
a_4	0.04347	0.06128	0.003649
a_5	-0.05412	-0.06997	0.01622
a_6	0.02642	0.03333	-0.01642
a_7	0.008946	-0.01044	0.01418
a_8	-0.009005	0.01131	-0.0152
b_1	-0.07725	-0.1169	-0.07103
b_2	0.01466	0.04827	-0.02544
b_3	0.004295	-0.02247	0.03135
b_4	-0.06679	-0.02642	-0.05162
b_5	0.05679	0.01599	0.05005
b_6	-0.01878	-0.0002684	-0.02426
b_7	0.01869	0.0136	-0.001858
b_8	-0.01888	-0.01632	0.0148

2.2 Blood Parametric Assumptions and Arterial Properties at Varying Physiological Conditions

The typical value for blood dynamic viscosity μ and its density ρ for human cardiovascular system is 0.0035 Ns/m^2 and 1060 kg/m^3, respectively [24]. The heart rate HR of the cardiovascular system used in the study is set at a constant value of 75 beat per minute (BPM) throughout the physiological conditions [25]. Specifically, the studied region of artery is at common carotid artery (CCA) where the blood supply carried from the heart to the neck and head [26]. The artery have a length L about 19.25 cm [27]. However, the thickening of the artery as the arterial blood pressure increases had cause the artery to become a little bit stenosed and the inner radius R_i of the lumen become reduced [28–30]. Based on the previous studies by Polak *et al.,* [31] and Casiglia *et al.,* [32], the thickness *h* of CCA in NBP, PH and HS1 conditions are 0.39 mm, 0.463 mm and 0.5 mm, respectively. The normotensive R_i of CCA in NBP condition is 3.1 mm [33]. For hypertensive conditions of PH and HS1, the radius is decreased by the increased thickness which obtaining the R_i value about 3.027 mm and 2.99 mm, respectively. For an arterial property of modulus elasticity E, a study by Messas *et al.,* has shown that the E value increases as the blood pressure increased [34]. According to the mean values for the static incremental modulus of carotid artery by Bergel, the MAP from the NBP to PH condition has an increasing E value about 20.6%. Meanwhile, the MAP from NBP to HS1 condition shows an increasing E value about 63.03% [35]. Normotensive condition of NBP has been shown to have an E value about 0.4 MPa [27]. Therefore, PH and HS1 conditions obtained an E value about 0.4824 MPa and 0.6521 MPa, respectively. Thus, Table 2 summarizes the obtained parameters used for the Windkessel model.

Table 2
Parameters for the Windkessel Model at Different Physiological Condition

Parameter	Physiological condition		
	NBP	*PH*	*HS1*
μ (Ns/m^2)	0.0035		
ρ (kg/m^3)	1060		
HR (BPM)	75		
L (mm)	192.5		
R_i (mm)	3.100	3.027	2.990
h (mm)	0.390	0.463	0.500
P_s (mmHg)	117	124	148
P_d (mmHg)	71	81	96
MAP (mmHg)	86.333	95.333	113.333
E (MPa)	0.4000	0.4824	0.6521

2.3 Systole Period

The mathematical model of 4-element Windkessel is started by calculating the systole period T_s of the blood pressure waveform. Based on a study by Catanho *et al.,* [7], the systole period is computed from the time of cardiac cycle T_c as follows:

$$T_c = \frac{60}{HR} \tag{3}$$

$$T_s = \frac{2}{5} T_c \tag{4}$$

2.4 Cardiac Output

Then, the cardiac output CO (L/min) of CCA is calculated as shown in Eq. (5) where SV (mL/beat) represents stroke volume by CCA [36]. The value of CO is able to identify of how much the blood flow rate produced by CCA.

$$CO = (1000 * SV) \times HR \tag{5}$$

SV is obtained by integrating the multiplication of the velocity waveform Fourier series $V(t)$ and the lumen cross-sectional area A of CCA as shown in Eq. (6). It is due to the area under the graph of blood flow rate waveform represents the volume of the blood per cardiac cycle [37]. Thus, the multiplication of $Q(t)$ is shown as in Eq. (7) while A is obtained through Eq. (8).

$$SV = \int_0^{T_c} Q(t)\, dt \tag{6}$$

$$Q(t) = A \times \left[a_0 + \sum_{n=1}^{8} a_n \cos(n(t - T_c)\omega) + \sum_{n=1}^{8} b_n \sin(n(t - T_c)\omega) \right] \tag{7}$$

$$A = \pi \mathrm{R}_{\mathrm{i}}^{2} \tag{8}$$

2.5 Womersley Number

Womersley number α is then calculated to obtain the Fry parameters which used in further computation. The Womersley number is a dimensionless parameter which represents a ratio of transient to viscous forces that calculated as shown in Eq. (9) where ω_{HR} is an angular velocity of heartbeat [24]. The ω_{HR} is yielded from Eq. (10) where f is the frequency (Hz) of the heartbeat. Meanwhile, f is a conversion from HR by using Eq. (11).

$$\alpha = \mathrm{R}_{\mathrm{i}} \left(\sqrt{\frac{\omega_{HR} \rho}{\mu}} \right) \tag{9}$$

$$\omega_{HR} = 2\pi f \tag{10}$$

$$f = \frac{\mathrm{HR}}{60} \tag{11}$$

2.6 Fry Parameters

Fry parameters consisting of resistance coefficient c_v and inertance coefficient c_u are important to analog the fluid parameters as the electrical circuit parameters. These Fry parameters are dependent to the Womersley number. Therefore, c_v and c_u are obtained from the curve of Womersley solution as shown in Figure 6 [24].

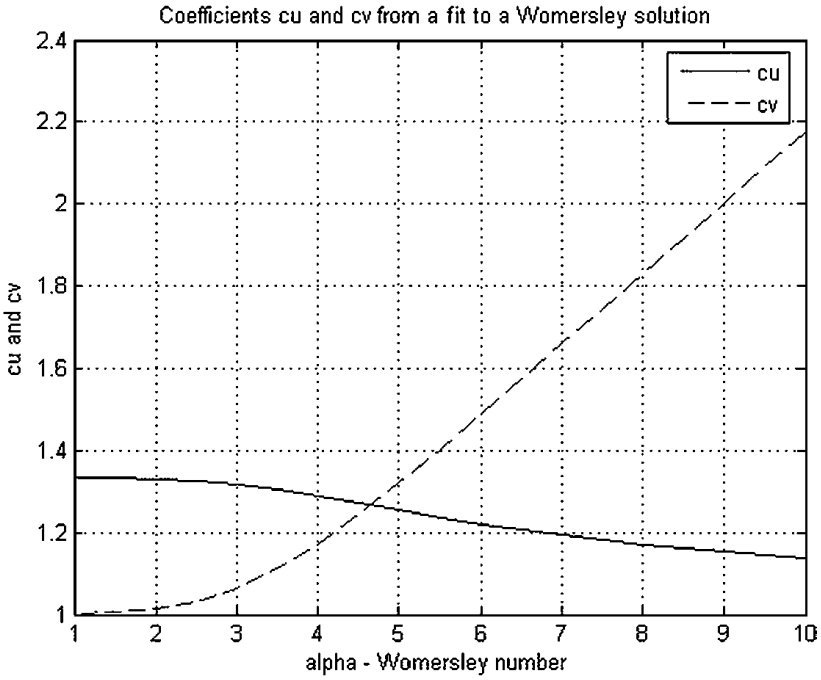

Fig. 6. Curve of Womersley solution in obtaining Fry parameters [24]

2.7 Arterial Resistance

The arterial resistance R_V (mmHg/cm^3/s) is a blood flow resistance encountered by the specific blood vessel which is CCA. R_V is calculated by using Eq. (12) [24].

$$R_V = \mathrm{L}\left(c_v \frac{8\mu}{\pi \mathrm{R_i}^4} \right) \tag{12}$$

2.8 Arterial Inductance

The arterial inductance L_V (mmHg/cm^3/s^2) represents the inertia of the blood flow in CCA. Thus, the L_V value is obtained by using Eq. (13) [24].

$$L_V = \mathrm{L}\left(c_u \frac{\rho}{\pi \mathrm{R_i}^2} \right) \tag{13}$$

2.9 Arterial Capacitance

The arterial capacitance C_V (cm^3/mmHg) represents the compliance of the blood vessel which is CCA. The C_V value is yielded from Eq. (14) [38].

$$C_V = \frac{3\pi \mathrm{R_i}^3 \mathrm{L}}{2\mathrm{E}h} \tag{14}$$

2.10 Peripheral Resistance

The peripheral resistance R (mmHg/cm^3/s) refers to the encountered resistance by the blood flow throughout the systemic arterial system. This parameter is obtained using Eq. (15) [39].

$$R = \left(\frac{60}{1000} \right) * \frac{\mathrm{MAP}}{\mathrm{CO}} \tag{15}$$

2.11 Arterial and Terminal End Load Impedances

As shown in Figure 2, the resistance R in 2-element equals to the summation of resistance R_1 and R_2 in 3-element as well as 4-element Windkessel models, which specifically shown in Eq. (16). The distribution of the resistances can be identified by matching the arterial impedance Z_V and the terminal end load impedance Z_e as displayed in Eq. (17). Z_V and Z_e are defined by the equations of Eq. (18) and Eq. (19), respectively where j is the imaginary number [24]. Besides, the capacitance of the terminal end load C_L (mmHg/cm^3/s) could also be determined.

$$R = R_1 + R_2 \tag{16}$$

$$Z_V = Z_e \tag{17}$$

$$Z_V = \left(\frac{R_V + j\omega L_V}{j\omega C_V} \right)^{1/2} \tag{18}$$

$$Z_e = R_1 + \frac{R_2 \left(1 - j\omega R_2 C_L\right)}{1 + R_2{}^2 C_L{}^2 \omega^2} \tag{19}$$

The arterial impedance Z_V in Eq. (18) yields the answer in the form of X_V+Y_Vj where X_V is the real unit of Z_V and Y_V is the imaginary unit of Z_V. Meanwhile, R_2 in Eq. (19) is replaced with $R-R_1$ and split into the form of real and imaginary units as shown in Eq. (20).

$$Z_e = R_1 + \frac{R - R_1}{1 + \left(R - R_1\right)^2 C_L{}^2 \omega^2} - \frac{\omega \left(R - R_1\right)^2 C_L}{1 + \left(R - R_1\right)^2 C_L{}^2 \omega^2} j \tag{20}$$

As Z_e is expanded into complex number, the real unit of Eq. (20) is matched with X_V while the imaginary unit of Eq. 20 is matched with Y_Vj as seen in Eq. (21) and Eq. (22), respectively.

$$X_V = R_1 + \frac{R - R_1}{1 + \left(R - R_1\right)^2 C_L{}^2 \omega^2} \tag{21}$$

$$Y_V j = - \frac{\omega \left(R - R_1\right)^2 C_L}{1 + \left(R - R_1\right)^2 C_L{}^2 \omega^2} j \tag{22}$$

The values of C_L, R_1 and R_2 are obtained by performing simultaneous equations of Eq. (21) and Eq. (22).

2.12 4-Element Windkessel Model

In the present study, an electrical circuit diagram by Catanho *et al.,* as shown in Figure 7 is used in the 4-element Windkessel model. Therefore, the mathematical model is as seen in Eq. (23) [7].

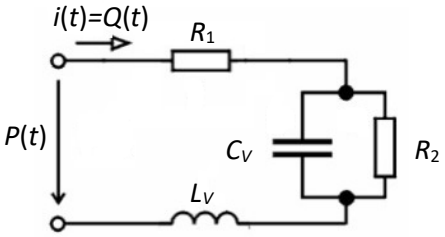

Fig. 7. An analogous electrical circuit of 4-element Windkessel model [7]

$$\left(1 + \frac{R_1}{R_2}\right) i(t) + \left(R_1 C_V + \frac{L_V}{R_2}\right) \frac{di(t)}{dt} + L_V C_V \frac{d^2 i(t)}{dt^2} = \frac{P(t)}{R_2} + C_V \frac{dP(t)}{dt} \tag{23}$$

Then, Eq. 23 is re-organized as shown in Eq. (24). By initializing the condition of $P(t)$ in Eq. (24) at MAP, Eq. (24) is solved using MATLAB Ordinary Differential Equations (ODE) solver.

$$\frac{dP(t)}{dt}=\left(\frac{R_2+R_1}{R_2C_V}\right)i(t)+\left(R_1+\frac{1}{C_VR_2}\right)\frac{di(t)}{dt}+L_V\frac{d^2i(t)}{dt^2}-\frac{P(t)}{C_VR_2} \tag{24}$$

2.13 Augmentation Index of Blood Pressure Waveform in CCA

The augmentation index (*AI*) is a measure of the wave reflection that indicates the arterial stiffness. Besides, *AI* also plays the main role as an indicator to the risk of cardiovascular disease. The *AI* value can be obtained by using Eq. (25) where *P*1 is the first systolic pressure while *P*2 represents the second systolic pressure while *PP* represents pulse pressure [22, 40].

$$AI=\frac{|P2-P1|}{PP}\times 100\% \tag{25}$$

2.14 Measured Blood Pressure Waveform by Previous Studies

There are two measured data of blood pressure waveform in carotid artery for adult which firstly by Nichols *et al.,* and secondly by Kingwell *et al.,* as shown in Figure 8 [41, 42]. The simulated data is compared with the measured data based on the relative error E_r of their standard deviations. The relative error is calculated as seen in Eq. (26) where d_{4WK} represents the numerical standard deviation while d_M represents the standard deviation of the measured data.

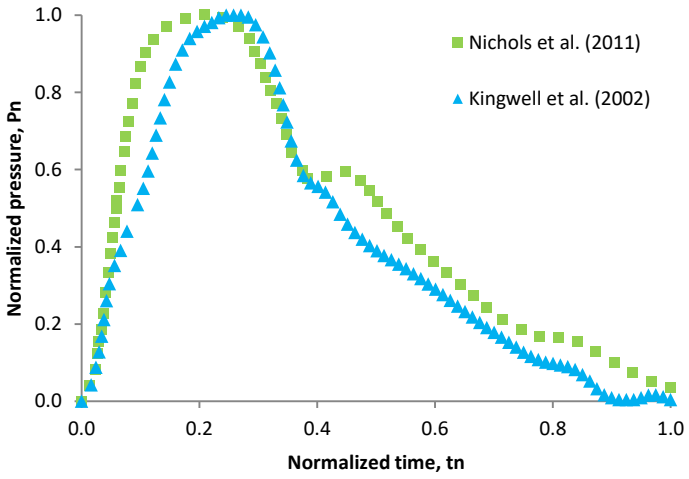

Fig. 8. Measured blood pressure waveform in carotid artery for adult [41,42]

$$Er=\left|\frac{d_{4WK}-d_M}{d_M}\right|\times 100\% \tag{26}$$

3. Results

3.1 Different Initializations of the Simulated Blood Pressure Waveform

As the MATLAB ODE solver needs the initial value of the blood pressure P_0, an assumption has to be made for a stable continuous cardiac cycle of the blood pressure. Figure 9 has shown a different pattern of blood pressure waveform during its first cycle using P_0 equals to 0 mmHg and 86.333 mmHg. Figure 9(a) displays an inaccurate of blood pressure where the first cycle started at negative values. Meanwhile, Figure 9(b) shows the cardiac cycles using 86.333 mmHg from the MAP value for the P_0 seems to be accurate and stable right at the starting point. Besides, the first cycle of the blood pressure waveform using MAP as the P_0 shows similar pattern with the other cycles.

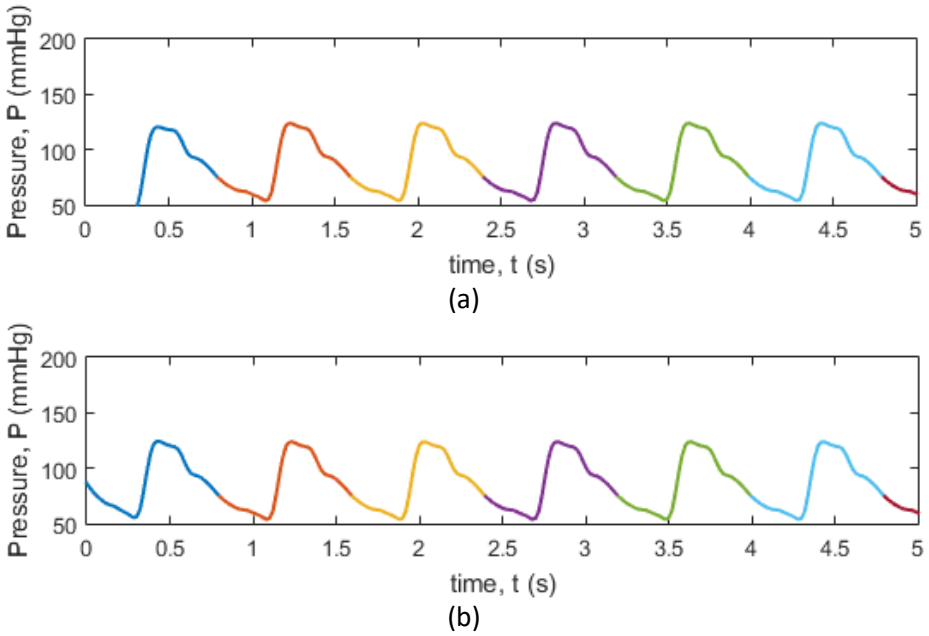

Fig. 9. Blood pressure waveform that initialized at (a) P_0 = 0 mmHg and (b) P_0 = 86.333 mmHg. Each color of the blood pressure waveform represents each of the cardiac cycle

3.2 Validation of Simulated Blood Pressure Waveform

As shown in Figure 10, the simulated Windkessel model of the present study has an E_r with the measured data by Nichols *et al.,* [41] about 6.45% while Kingwell *et al.,* [42] about 2.51%. The comparison is made in the NBP physiological condition of carotid artery. Since the errors between the numerical and the measured data are small, the Windkessel model of the present study is considered as acceptable and valid. Therefore, the present study is furthered with the analysis of hypertensive physiological conditions of carotid artery.

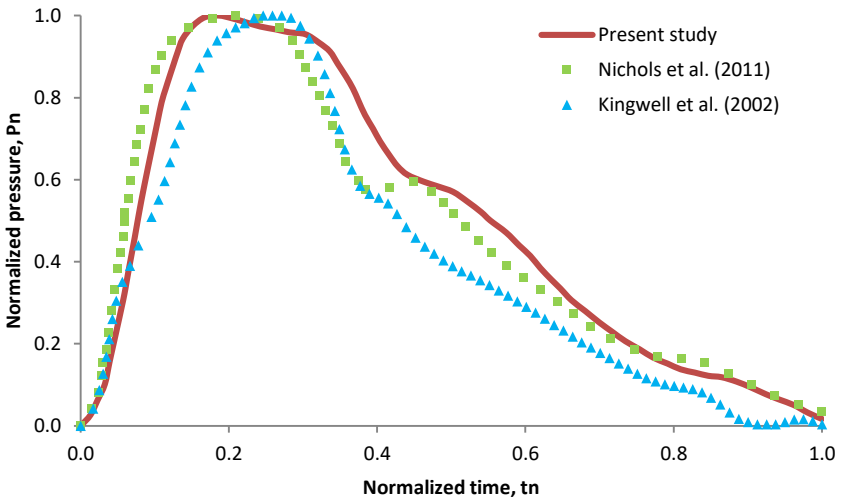

Fig. 10. Simulated Windkessel model and the measured blood pressure waveforms [41,42]

3.3 Blood Pressure Waveform of CCA at Specific Physiological Condition

The increasing order of blood physiological condition from NBP to HS1 gives an increase in resistance, decrease in capacitance and decrease in inductance. As shown in Table 3, R value increased from 7.6706 mmHg/cm^3/s for NBP to 9.8052 mmHg/cm^3/s for HS1 condition. It means that the flow resistance encountered by the blood throughout the systemic arterial system from NBP to HS1 condition increased about 27.83%. For R_V, the flow resistance in CCA increased from NBP to HS1 condition about 13.15%. This result is in an agreement with the study by Stergiopulos *et al.,* displaying the peripheral resistance increases as the blood pressure increases [40]. On the other hand, the arterial compliance C_V by NBP, PH and HS1 conditions show to have the value about 0.0231, 0.0150 and 0.0099 cm^3/mmHg, respectively. It indicates that the elasticity of CCA is dropped from NBP to HS1 about 57.14%. This decrement has proven that the thickening of an arterial wall to be increased as the blood pressure rise [28–30]. Meanwhile, the arterial inductance shows not much difference although the values are at increasing order. The L_V by NBP, PH and HS1 conditions showed CCA to have the value about 0.064, 0.0673 and 0.0691 mmHg/cm^3/s^2, respectively, which shown to have an increment about 7.99%. It has proven that the high blood physiological condition give small increment in term of the blood flow inertia.

Table 3
The Calculated Values of Electrical Parameters by each Physiological Condition

Electrical Parameter	Physiological condition		
	NBP	*PH*	*HS1*
R (mmHg/cm^3/s)	7.6706	8.3917	9.8052
R_1 (mmHg/cm^3/s)	1.6753	2.1278	2.6511
R_2 (mmHg/cm^3/s)	5.9953	6.2638	7.1542
R_V (mmHg/cm^3/s)	0.1795	0.1947	0.2031
C_V (cm^3/mmHg)	0.0231	0.0150	0.0099
L_V (mmHg/cm^3/s^2)	0.0640	0.0673	0.0691

The obtained electrical parameters by each blood physiological condition displays a specific pattern blood flow waveform as shown in Figure 11, Figure 12 and Figure 13. The blood flow rate and the simulated pressure waveform of Figure 11 represent NBP condition, Figure 12 represent PH condition while Figure 13 represent HS1 condition. All the blood pressure waveforms are seen to be varied according to the flow rate waveform at full three cardiac cycles.

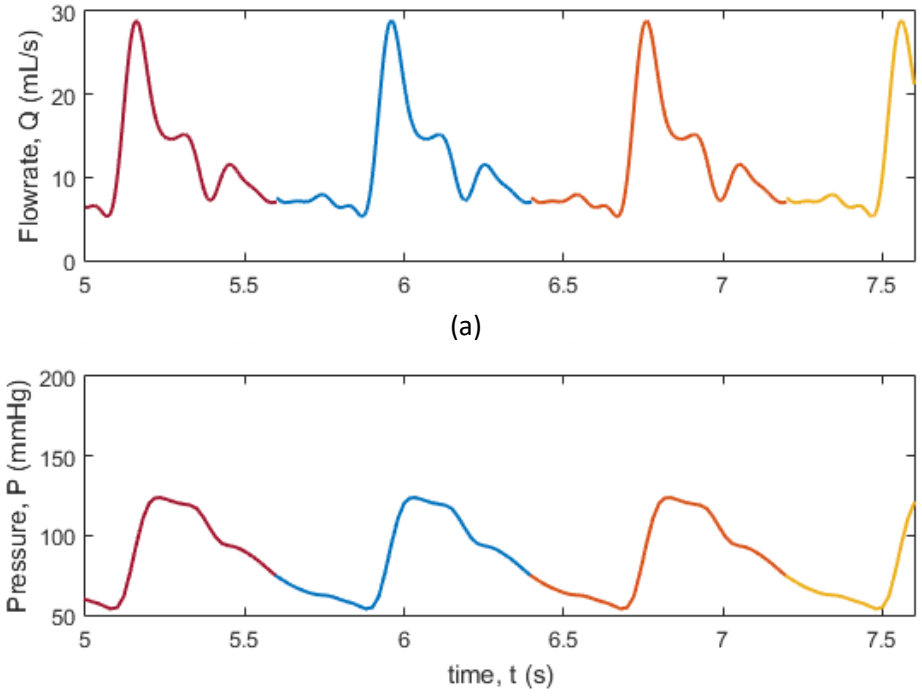

Fig. 11. (a) Blood flow rate and (b) simulated pressure waveform of CCA for NBP condition. The color of the curve represents different cardiac cycle

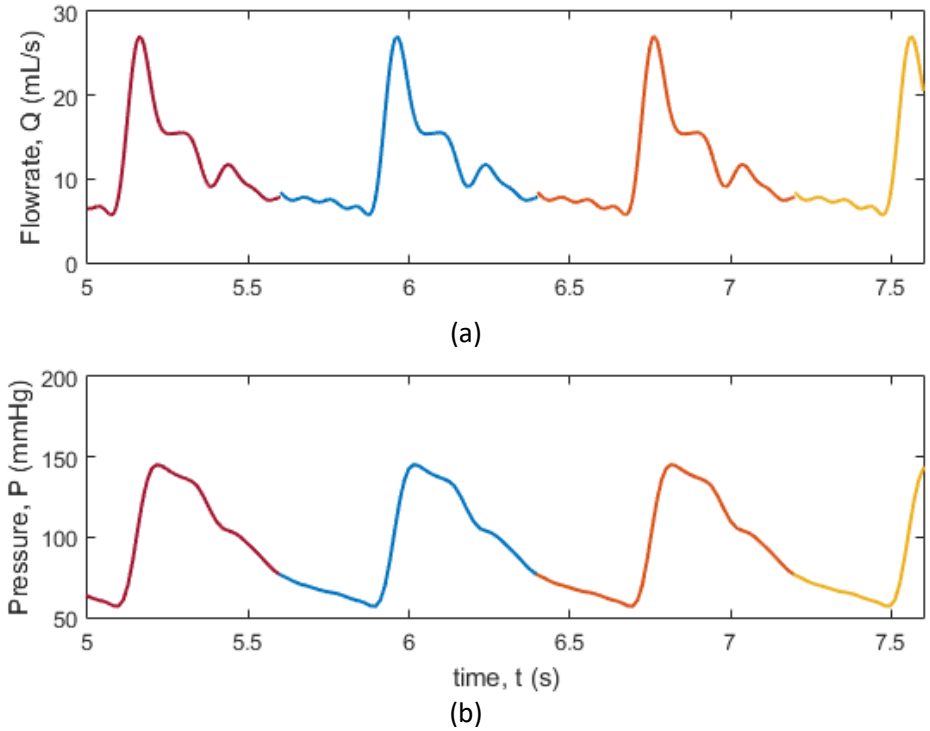

Fig. 12. (a) Blood flow rate and (b) simulated pressure waveform of CCA for PH condition. The color of the curve represents different cardiac cycle

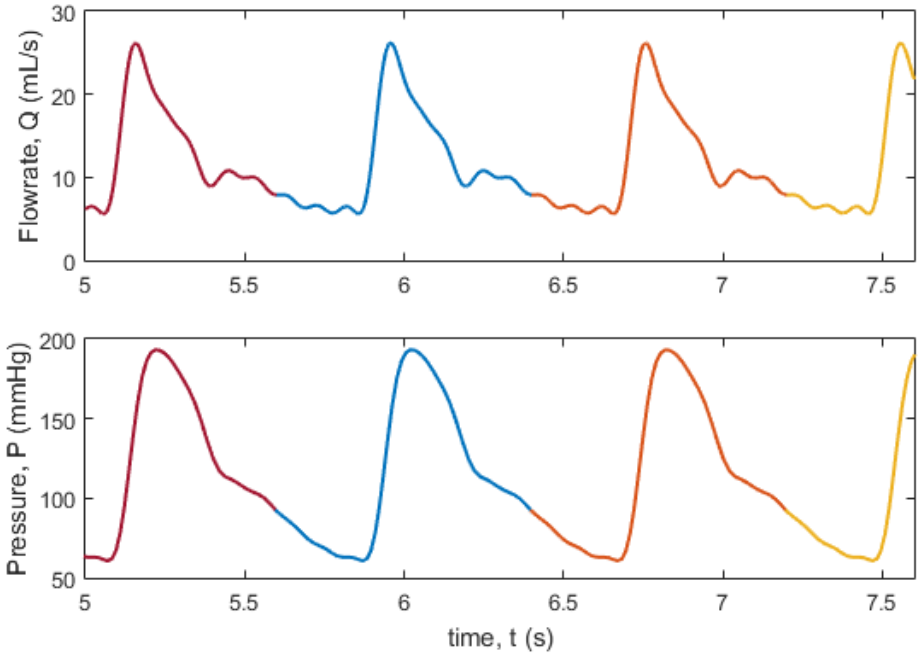

Fig. 13. (a) Blood flow rate and (b) simulated pressure waveform of CCA for HS1 condition. The color of the curve represents different cardiac cycle

3.4 Cardiac Activity of Blood Pressure Waveform at Different Physiological Conditions

The systole period of the simulated blood pressure waveforms averagely start from 0.28 s to 0.62 s while the other time cardiac cycle shows a diastolic period as shown in Figure 14. Specifically, the diastolic pressure by each of the physiological condition in NBP is shown to have about 53.859 mmHg at 0.28 s, PH is shown to have about 56.956 mmHg at 0.3 s while HS1 is shown to have about 60.713 mmHg at 0.27 s. As the heart contracts, the blood flow is ejected rapidly from the heart to CCA. The heart contraction has caused the first systolic pressure in CCA by NBP condition shows 123.798 mmHg, PH condition shows 145.115 mmHg while HS1 condition shows 193.146 mmHg at an average cardiac cycle of 0.42 s. The physiological condition from NBP to PH is demonstrated to have an increment of first systolic pressure about 17.22% while from NBP to HS1 demonstrated the increment about 56.02%. As the rejection is reduced, the pressure waves are reflected causing the second systolic pressure to be identified. The second systolic pressure by NBP condition is 116.963 mmHg, PH condition is 131.945 mmHg and HS1 condition is 159.817 mmHg. The duration of the reflected wave is averagely 0.12 s as the reflection ends exactly at 0.54 s. Then, the ejection process stops the blood flow at 0.62 s where a dicrotic notch is spotted. As the diastole period begins, the pressure decreases gradually which caused by the inflow from CCA to the heart.

The pulse pressures of CCA in NBP, PH and HS1 condition are shown at the values about 69.939 mmHg, 88.159 mmHg and 132.433 mmHg, respectively. Meanwhile, the pulse pressures of the heart in NBP, PH and HS1 conditions are 46 mmHg, 43 mmHg and 52 mmHg, respectively. This comparison between the obtained pulse pressures in CCA and the heart has proven that the enlargement of the propagated wave is in agreement with a study by Ohno *et al.,* [21] which also showing the increasing of pulse pressure from the central aorta to the peripheral artery. From the obtained first systolic, second systolic and pulse pressures, the augmentation index by NBP condition is shown to have *AI* value about 9.77%, PH condition shows 14.94% while HS1 condition shows 25.17%. On the other hand, Weber *et al.,* obtained *AI* on healthy artery about 11.7% while the artery with cardiovascular disease about 17.2% [43]. Meanwhile, the *AI* by NBP condition of the present study is shown to have

lower value than 11.7% while the *AI* by the HS1 condition is shown to have higher value than 17.2%. Based on the benchmark by the previous study, it is proven that the simulated pressure waveform by NBP condition in CCA is in agreement with the normotensive state. Since hypertension is associated with the cardiovascular disease, the pressure waveform of HS1 in CCA is acceptable as the hypertensive condition. However, the *AI* by the simulated pressure waveform of PH condition falls between 11.7% and 17.2%. Thus, the PH condition only shows the elevated blood pressure waveform from the normotensive state which has a high risk to the cardiovascular disease of hypertension.

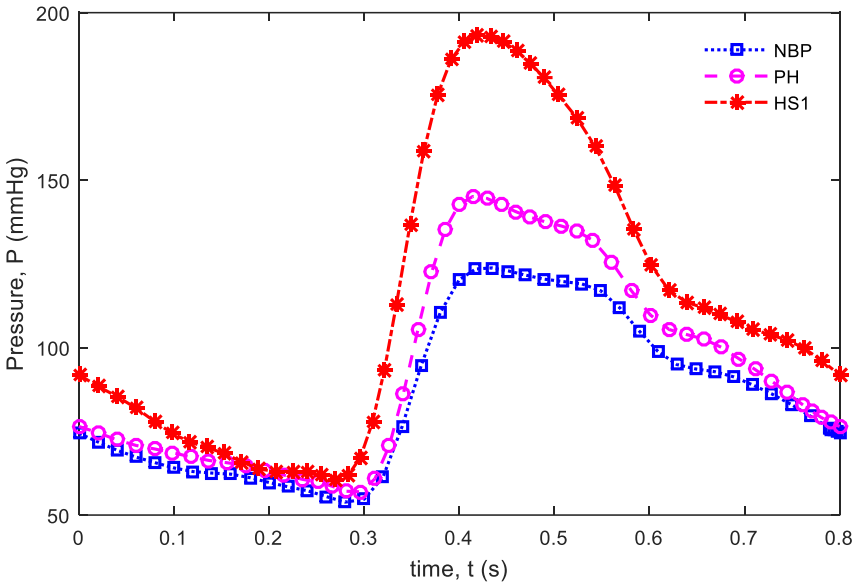

Fig. 14. Simulated blood pressure waveforms in CCA at NBP, PH and HS1 conditions

4. Conclusions

The electrical parameters of Windkessel model has shown that physiological of blood in CCA from normotensive to hypertensive condition produced an increment of peripheral resistance about 27.83%, a decrement of arterial capacitance about 57.14% and an increment of arterial inductance about 7.99%.These electrical parameters have shown the blood pressure waveform to have AI in NBP, PH and HS1 conditions about 9.77%, 14.94% and 25.17%, respectively. As the results shown are acceptable compared with the previous studies, the simulated blood pressure waveforms are reliable in describing the activity that happens on each cardiac cycle.

Although the mathematical model used in 4-element Windkessel model is simple, there are too many properties that need to be considered so data are synchronize in terms of blood pressure, arterial circumstances and age. On the other hand, the mathematical model is very useful to those who study the blood flow invasively through computational fluid dynamic method.

Acknowledgement
Authors acknowledge Ministry of Education, Malaysia and Universiti Tun Hussein Onn Malaysia (UTHM) for sponsoring this project financially through Fundamental Research Grant Scheme (FRGS) 1/2016 Vot. 1529.

References

[1] Barnea, Ofer. "Open-source programming of cardiovascular pressure-flow dynamics using SimPower toolbox in Matlab and Simulink." *The Open Pacing, Electrophysiology & Therapy Journal* 3, no. 1 (2010): 55-59.
[2] Abdi, M., A. Karimi, M. Navidbakhsh, K. Hassani, and S. Faghihi. "RETRACTED: Modeling of cerebral aneurysm using equivalent electrical circuit (Lumped Model)." *Perfusion* 29, no. 2 (2014): 142-152.
[3] Olufsen, Mette S. and Ali Nadim. "On Deriving Lumped Models for Blood Flow and pressure in the Systemic Arteries, " *Math. Biosci. Eng.* 1, no. 1 (2004): 61–80.
[4] Basri, Adi Azriff, Shah Mohammed Abdul Khader, Cherian Johny, Raghuvir Pai, Muhammad Zuber, Kamarul Arifin Ahmad, and Zanuldin Ahmad. "Numerical Study of Haemodynamics Behaviour in Normal and Single Stenosed Renal Artery using Fluid–Structure Interaction." *Journal of Advanced Research in Fluid Mechanics and Thermal Sciences* 51, no. 1 (2018): 91-98.
[5] Mahmud, K. R., M. M. Rhaman, and A. K. Al Azad. "Numerical Simulation and Analysis of Incompressible Newtonian Fluid Flows using FreeFem++." *Journal of Advanced Research in Fluid Mechanics and Thermal Sciences* 26, no. 1 (2016): 1-19.
[6] Gerringer, Jesse W., Julie C. Wagner, Daniela Vélez-Rendón, and Daniela Valdez-Jasso. "Lumped-parameter models of the pulmonary vasculature during the progression of pulmonary arterial hypertension." *Physiological reports* 6, no. 3 (2018).
[7] Catanho, Marianne, Mridu Sinha, and Varsha Vijayan. "Model of aortic blood flow using the windkessel effect." *BENG 221–Mathematical Methods in Bioengineering* (2012).
[8] M.S.A. Paisal, S.F.S Adnan, I. Taib, A.E Ismail, M.K Abdullah, N. Nordin, S.M Seri and N. Darlis, "Flow Characteristics Near to Stent Strut Configurations on Femoropopliteal Artery", *IOP Conference Series: Materials Science and Engineering*, vol. 226, no. 1, 012147, 2017.
[9] B.A Mohd Atan, A.E Ismail, I. Taib and Z. Lazim, "A review on fracture prevention of stent in femoropopliteal artery", *IOP Conference Series: Materials Science and Engineering*, vol. 166, no. 1, 012006, 2017.
[10] M.S Amir Paisal, I. Taib and A.E Ismail, "Computational Analysis on Stent Geometries in Carotid Artery: A Review", *IOP Conference Series: Materials Science and Engineering*, vol. 166, no. 1, 012003, 2017.
[11] Z. Lazim, A.E Ismail, I. Taib and B.A Mohd Atan, "A review of stent's failure on patent ductus arteriosus", *IOP Conference Series: Materials Science and Engineering*, vol. 166, no. 1, 012007, 2017.
[12] Asrizan Kaha, Ishkrizat Taib, Muhammad Sufyan Amir Paisal, Ahmad Mubarak Tajul Arifin, Al Emran Ismail, Norzelawati Asmuin, Reazul Haq Abdul Haq, Surapong Chatpun, Takahisa Yamamoto, and Kahar Osman, "Lumped Parameter Modelling in Femoral Popliteal Artery for Normal and Severe Conditions", *International Journal of Integrated Engineering: Special issue 2018: Mechanical Engineering*, vol. 10, no. 5, pp. 193-203, 2018.
[13] Hamdan, A., F. Mustapha, K. A. Ahmad, A. S. Mohd Rafie, M. R. Ishak, and A. E. Ismail. "The effect of customized woven and stacked layer orientation on tensile and flexural properties of woven kenaf fibre reinforced epoxy composites." *International Journal of Polymer Science* 2016 (2016).
[14] Ismail, Al Emran, and M. A. Hassan. "Low velocity impact on woven kenaf fiber reinforced composites." In *Applied Mechanics and Materials*, vol. 629, pp. 503-506. Trans Tech Publications, 2014.
[15] Peña Pérez, Nuria. "Windkessel modeling of the human arterial system." Bachelor's thesis, 2016.
[16] Tenti, Giuseppe, Siv Sivaloganathan, and James M. Drake. "Mathematical modeling of the brain: Principles and challenges." *Neurosurgery* 62, no. 5 (2008): 1146-1157.
[17] Burattini, Roberto, and Paola Oriana Di Salvia. "Development of systemic arterial mechanical properties from infancy to adulthood interpreted by four-element windkessel models." *Journal of Applied Physiology* 103, no. 1 (2007): 66-79.
[18] Shimizu, Shuji, Dai Une, Toru Kawada, Yohsuke Hayama, Atsunori Kamiya, Toshiaki Shishido, and Masaru Sugimachi. "Lumped parameter model for hemodynamic simulation of congenital heart diseases." *The Journal of Physiological Sciences* 68, no. 2 (2018): 103-111.
[19] Stergiopulos, Nikos, Berend E. Westerhof, and Nico Westerhof. "Total arterial inertance as the fourth element of the windkessel model." *American Journal of Physiology-Heart and Circulatory Physiology* 276, no. 1 (1999): H81-H88.
[20] Salvi, Paolo. "Mean arterial pressure." In *Pulse Waves*, pp. 3-7. Springer, Milano, 2012.
[21] Ohno, Yoichi, Yoshihiko Kanno, and Tsuneo Takenaka. "Central blood pressure and chronic kidney disease." *World journal of nephrology* 5, no. 1 (2016): 90-100.
[22] da Fonseca, Lucas José Sá, Marco Antônio Mota-Gomes, and Luíza A. Rabelo. "Radial applanation tonometry as an adjuvant tool in the noninvasive arterial stiffness and blood pressure assessment." *World Journal of Cardiovascular Diseases* 4, no. 05 (2014): 225-235.
[23] Azhim, A., K. Sakagami, A. Ueno, Y. Kinouchi, and Y. Fukui. "Independent factors of flow velocity indices in common

carotid artery." In *World Congress on Medical Physics and Biomedical Engineering May 26-31, 2012, Beijing, China*, pp. 445-448. Springer, Berlin, Heidelberg, 2013.
[24] Waite, Lee, and Jerry Michael Fine. "Applied biofluid mechanics." (2007).
[25] Berkow, R. "Merck Research Laboratories." *The Merck Manual of Medical Information: Home Edition. Merck Research Laboratories, Whitehouse Station, New Jersey* (1997).
[26] Lin, P. H., Poi, M. J., Matos, J., Kougias, P., Bechara, C. and Changyi, C. "Schwartz's Principles of Surgery." *Tenth. New York City: McGraw-Hill Education*, (2015).
[27] Kashefi, A., M. Mahdinia, B. Firoozabadi, M. Amirkhosravi, G. Ahmadi, and M. S. Saidi. "Multidimensional modeling of the stenosed carotid artery: A novel CAD approach accompanied by an extensive lumped model." *Acta Mechanica Sinica* 30, no. 2 (2014): 259-273.
[28] Su, Ta-Chen, Jiann-Shing Jeng, Kuo-Liong Chien, Fung-Chang Sung, Hsiu-Ching Hsu, and Yuan-Teh Lee. "Hypertension status is the major determinant of carotid atherosclerosis: a community-based study in Taiwan." *Stroke*32, no. 10 (2001): 2265-2271.
[29] Litwin, Mieczysław, Justyna Trelewicz, Zbigniew Wawer, Jolanta Antoniewicz, Aldona Wierzbicka, Pawel Rajszys, and Ryszard Grenda. "Intima-media thickness and arterial elasticity in hypertensive children: controlled study." *Pediatric nephrology* 19, no. 7 (2004): 767-774.
[30] Lábrová, R., N. Honzíková, E. Maderova, P. Vysocanová, Z. Nováková, E. Závodná, B. Fiser, and B. Semrád. "Age-dependent relationship between the carotid intima-media thickness, baroreflex sensitivity, and the inter-beat interval in normotensive and hypertensive subjects." *Physiological research* 54, no. 6 (2005): 593-600.
[31] Polak, Joseph F., Sharina D. Person, Gina S. Wei, Ayleen Godreau, David R. Jacobs Jr, Anita Harrington, Stephen Sidney, and Daniel H. O'Leary. "Segment-specific associations of carotid intima-media thickness with cardiovascular risk factors: the Coronary Artery Risk Development in Young Adults (CARDIA) study." *Stroke* 41, no. 1 (2010): 9-15.
[32] Casiglia, Edoardo, Paolo Palatini, Santina Da Ros, Valeria Pagliara, Massimo Puato, Francesca Dorigatti, and Paolo Pauletto. "Effect of blood pressure and physical activity on carotid artery intima–media thickness in stage 1 hypertensives and controls." *American journal of hypertension* 13, no. 12 (2000): 1256-1262.
[33] Perktold, Karl, Michael Resch, and Reinfried O. Peter. "Three-dimensional numerical analysis of pulsatile flow and wall shear stress in the carotid artery bifurcation." *Journal of Biomechanics* 24, no. 6 (1991): 409-420.
[34] Messas, E., M. Pernot, and M. Couade. "Arterial wall elasticity: state of the art and future prospects." *Diagnostic and interventional imaging* 94, no. 5 (2013): 561-569.
[35] Bergel, D.H., 1961. "The static elastic properties of the arterial wall. " *The Journal of physiology*, *156*(3), pp.445-457.
[36] Taib, Ishkrizat. "Improvement of Haemodynamic Stent Strut Configuration for Patent Ductus Arteriosus Through Computational Modelling." PhD diss., Universiti Teknologi Malaysia, 2016.
[37] Piatti, Filippo, Francesco Sturla, Malenka M. Bissell, Selene Pirola, Massimo Lombardi, Igor Nesteruk, Alessandro Della Corte, Alberto CL Redaelli, and Emiliano Votta. "4D flow analysis of BAV-Related fluid-dynamic alterations: evidences of wall shear stress alterations in absence of clinically-relevant aortic anatomical remodeling." *Frontiers in physiology* 8 (2017): 441.
[38] Naik, Ketan B., and P. H. Bhathawala. "Mathematical modelling and simulation of human systemic arterial system." *Int J Eng Innovative Technol* 4, no. 1 (2014).
[39] Diroll, Anne, and Diana Hlebovy. "Inverse relationship between blood volume and blood pressure." *Nephrology Nursing Journal* 30, no. 4 (2003): 460-461.
[40] Stergiopulos, N. I. K. O. S., JEAN-JACQUES Meister, and N. I. C. O. Westerhof. "Determinants of stroke volume and systolic and diastolic aortic pressure." *American Journal of Physiology-Heart and Circulatory Physiology* 270, no. 6 (1996): H2050-H2059.
[41] Vlachopoulos, Charalambos, Michael O'Rourke, and Wilmer W. Nichols. *McDonald's blood flow in arteries: theoretical, experimental and clinical principles*. CRC press, 2011.
[42] Kingwell, Bronwyn A., and Christoph D. Gatzka. "Arterial stiffness and prediction of cardiovascular risk." *Journal of hypertension* 20, no. 12 (2002): 2337-2340.
[43] Weber, Thomas, Johann Auer, Michael F. O'Rourke, Erich Kvas, Elisabeth Lassnig, Robert Berent, and Bernd Eber. "Arterial stiffness, wave reflections, and the risk of coronary artery disease." *Circulation* 109, no. 2 (2004): 184-189.